Multiple Redox Modes in the Reversible Lithiation of High-Capacity, Peierls-Distorted Vanadium Sulfide

Sylvia Britto,[*] Michal Leskes,[*] Xiao Hua,[*] Claire-Alice Hébert,[§] Hyeon Suk Shin,[#] Simon Clarke,[††] Olaf Borkiewicz,[+] Karena W. Chapman,[+] Ram Seshadri,[‡] Jaephil Cho[†] and Clare P. Grey[*@]

[*]*Department of Chemistry, Lensfield Road, University of Cambridge, Cambridge CB2 1EW, United Kingdom*

[#]*Department of Chemistry and Department of Energy Engineering, Ulsan National Institute of Science and Technology, Korea*

[§]*College of Creative Studies, University of California, Santa Barbara, CA 93106, USA*

[+]*X-ray Science Division, Advanced Photon Source, Argonne National Laboratory, Illinois 60439, USA*

[‡]*Mitsubishi Chemicals Center for Advanced Materials Research Laboratory, University of California, Santa Barbara, CA 93106, USA*

[†]*Nano Energy Materials Lab, Interdisciplinary School of Green Energy, Ulsan National Institute of Science and Technology, Korea*

[††]*Department of Chemistry, University of Oxford, Inorganic Chemistry Laboratory, South Parks Road, Oxford, OX1 3QR, UK.*

[@]Corresponding author, cpg27@cam.ac.uk

Keywords: *lithium-ion battery, conversion mechanism, peierls distortion*

ABSTRACT

Vanadium sulfide VS_4 in the patronite mineral structure, is a linear chain compound comprising vanadium atoms coordinated by disulfide anions $[S_2]^{2-}$. ^{51}V NMR shows that the material, despite having V formally in the d^1 configuration, is diamagnetic, suggesting potential dimerization through metal-metal bonding associated with a Peierls distortion of the linear chains. This is supported by density functional calculations, and is also consistent with the observed alternation in V-V distances of 2.8 Å and 3.2 Å along the chains. Partial lithiation results in reduction of the disulfide ions to sulfide S^{2-}, including via an internal redox process whereby an electron from V^{4+} is transferred to $[S_2]^{2-}$ resulting in oxidation of V^{4+} to V^{5+} and reduction of the $[S_2]^{2-}$ to S^{2-} to form Li_3VS_4 containing tetrahedral $[VS_4]^{3-}$ anions. On further lithiation this is followed by reduction of the V^{5+} in Li_3VS_4 to form $Li_{3+x}VS_4$ (x=0.5-1), a mixed valent V^{4+}/V^{5+} compound. Eventually reduction to Li_2S plus elemental V occurs. Despite the complex redox processes involving both the cation and the anion occurring in this material, the system is found to be partially reversible between 0 and 3 V. The unusual redox processes in this system are elucidated using a suite of short range characterization tools including ^{51}V Nuclear Magnetic Resonance spectroscopy (NMR), S K-edge X-ray Absorption Near Edge Spectroscopy (XANES) and Pair Distribution Function (PDF) Analysis of X-ray data.

INTRODUCTION

The reversible reactions of insertion electrodes such as LiCoO$_2$[1] and graphite[2] in rechargeable Li ion batteries are frequently based on topotactic reactions where the layered structure of the host remains essentially intact as Li$^+$ ions diffuse in and out of the interlayer region during the redox process. Such a mechanism ensures easy reversibility and long cycle life. However the capacities of these materials are generally limited to 0.5 to 1 e$^-$ redox change per transition metal ion owing to the limited number of sites available in the interlayer region for the incorporation of lithium ions. Higher capacities may be achieved through materials that are capable of undergoing a wider change in oxidation states, thereby allowing for the accommodation of more than one Li ion per transition metal ion. Such a redox change would require that either the (i) host structure has novel architectures such as tunnel or framework structures with a greater number of potential sites for Li-ion incorporation as well as being stable in both the fully reduced and oxidized states or (ii) that the redox process involves a non-topotactic structural change in which the host electrode material breaks down to facilitate complete reduction of the redox-active metal ion to the elemental metal. The former strategy has been applied in materials such as the NASICON M$_2$(XO$_4$)$_3$ framework which are capable of accommodating reversibly up to 5 Li ions per formula unit, and up to 2-3 Li per transition metal ion.[3-5] Conversion electrodes based on transition metal oxides operate through the latter mechanism through a reaction that can be depicted as:

$$M_xX_y + ny\text{Li}^+ \rightarrow y\text{Li}_nX + xM \text{ [6]}$$
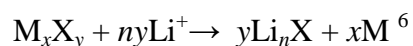
Such a reaction is not limited to oxides but can be extended to sulphides, nitrides, fluorides, pnictides, *etc.* Despite the high capacities achievable by conversion electrode materials, many of them suffer from a number of drawbacks such as poor reversibility, high coulombic inefficiencies and a large voltage hysteresis. Transition metal sulphides have been explored both as insertion electrodes, for example, TiS$_2$ and TaS$_2$[7] as well as as conversion electrodes such as FeS$_2$, NiS$_2$ and CoS$_2$.[8,9] The latter sulfides contain [S$_2$]$^{2-}$ disulfide anions and crystallize in the pyrite crystal structure. FeS$_2$, in particular, exhibits excellent reversibility at high temperatures and has, therefore, been explored in high temperature batteries; however, it shows poor reversibility at ambient temperatures .[6,9]

Recently, it has been shown that the compound VS$_4$,[10] with a unique linear chain structure, exhibits a remarkably high capacity of ~730 mAh/g at rates as high as 4C with good capacity retention over ~50 cycles.[11,12] Vanadium sulfide was discovered as the mineral patronite in 1906. The crystal structure, determined in 1964,[13] revealed that the material is comprised of V^{4+} ions coordinated to sulphur dimers forming linear chains extending along the *c*-axis (Figure 1). No attempt was made however to link the crystal structure of the material to its electronic properties, apart from some early suggestions[14-16],that VS$_4$ appeared to display a Peierls distortion. Recently, it has been suggested from DFT calculations that the material exhibits a band gap of ~1.0 eV.[12] The open channels in-between the chains offer potential sites for topotactic Li insertion. The detailed mechanism for the redox process however is not well understood. The reasons for the facile reversibility in this system are also not clear. Previous reports[11] suggest that the reversibility in this system is due to the oxidation

of the Li_2S formed at the end of discharge to form S, so that beyond the first cycle, the electrochemistry is suggested to be akin to that of a Li-S battery. Insights into the mechanism of electrochemical behaviour of conversion materials is challenging owing to the x-ray amorphous nature of the intermediates and products formed during charge/discharge of the battery.

In this contribution, we use density functional theory-based calculations of the electronic structure to establish the Peierls distortion and the nature of the diamagnetic, insulating ground state of the VS_4. We then employ a suite of structural characterization tools such as pair distribution function (PDF) analysis, solid state nuclear magnetic resonance spectroscopy (ssNMR) and S K-edge X-ray absorption near-edge spectroscopy (XANES) to examine the electrochemical behaviour in this compound and the mechanisms underpinning the structural transformation. Both [6]Li and [51]V NMR spectroscopy are used. [51]V is a spin 7/2 nucleus with a natural abundance of 99.75 % and a relatively small quadrupolar moment, with a chemical shift range that is extremely sensitive to local structure.[17] The NMR and XANES spectra are compared with model compounds, to help assign specific spectral signatures to different local structures. A rich redox chemistry involving both the anion and the cation is identified, an understanding of which throws valuable insights into the role that metal-ligand covalency plays in controlling the reversibility of such systems.

EXPERIMENTAL AND THEORETICAL METHODS

Electronic Structure Calculations. Density functional theory-based electronic structure calculations on VS_4 were performed using the Vienna Ab-initio Simulation Package (VASP version 5.2)[18, 19, 20, 21] with the wavefunctions described by a plane-wave basis set and the ionic potentials described by projector augmented wave (PAW) potentials of Blöchl.[22, 23] The energy cut off for the plane waves was set to 500 eV and a grid of at least 100 k-points was used for all calculations. The energy convergence criteria was 10^{-5} eV. Ground state electronic structures were relaxed with Perdew-Burke-Ernezhof generalized gradient approximated (GGA-PBE)[24] functionals by optimizing the position of sulfur atoms around the vanadium chains, keeping the V-V bond length fixed. Heyd-Scuseria-Ernzerhof (HSE)[25] screened hybrid functionals were also used to calculate the gap of the dimer structure, as HSE is known to better estimate band gaps than PBE. Structures were visualized in VESTA.[26]

Materials Preparation. VS_4-reduced graphene oxide (rGO) powder was prepared using the synthesis procedure described in a previous paper.[12] Briefly, GO was prepared from natural graphite powder by the Hummer's Method.[27] The GO solution (5 mg/mL) was added to a mixture of sodium orthovanadate and thioacetamide to make a total volume of 120 mL. The solution was transferred to a 150-mL Teflon-lined stainless steel autoclave and heated up to 160°C for 24 h. The product was then filtered, washed with DI water and dried in vacuum at 60°C for 6 h. K_3VS_4 and $LiVS_2$, which were used as model compounds for the XANES measurements, were prepared by a sealed tube method. K_3VS_4 was synthesized by carefully mixing together stoichiometric amounts of K_2S, V, and S and heating the resulting mixture in

a sealed tube at 650°C for 20 hours. $LiVS_2$ was prepared by grinding together stoichiometric quantities of Li_2S, V and S and heating the resulting mixture at 750°C for 20 hours. The other model compounds, Li_2S and S, were sourced from Sigma-Aldrich.

Electrochemical Characterization. The electrodes were made of VS_4-rGO composite (rGO 3% by weight) Ketjen Black and polyvinylidine fluoride (PVDF) binder in a weight ratio of 80:10:10 cast onto copper foil. Coin-type half cells containing the VS_4-rGO films, Li metal as counter electrode, borosilicate glass fibre separator (Whatman) and electrolyte [(1M $LiPF_6$ in ethylene carbonate (EC) /dimethyl carbonate (DMC) 1:1 ((v/v)Merck)] were assembled in an argon filled glove box. The batteries were cycled between $0 – 3.0$ V at rates of C/5 or C/10 in galvanostatic mode in an Arbin battery cycler. For ex-situ characterization, after cycling to a specific cutoff potential, the films were extracted from the coin cells, rinsed with dimethyl carbonate solvent and dried in a vacuum. The electrode material was scraped off the film for solid state NMR, ex-situ PDF and XANES measurements.

X-ray Diffraction (XRD). Laboratory powder diffraction was carried out using an Empyrean powder diffractometer equipped with a Cu source (Cu Kα = 1.5418 Å). *In-situ* XRD was collected at beamline 11-BM (λ = 0.4137 Å) of the Advanced Photon Source (APS) at Argonne National Laboratory. For in-situ XRD measurements, electrode pellets were prepared by mixing the VS_4-rGO nanocomposite with "Super P" carbon, (Alfa Aesar), carbon black, and polytetrafluoroethylene (PTFE) binder (Sigma-Aldrich) in the mass ratio 6:1:1:2. The pellets were assembled into the AMPIX electrochemical cell[28] with a glass fibre separator (Whatman GF/A), Li metal foil and liquid electrolyte (1M $LiPF_6$ in 3:7 v:v (EC:DMC) from Tomiyama Pure Chemical Industries) within an argon glovebox. The electrolyte and binder used in the in-situ XRD experiments were different from those used for the ex-situ measurements, as the in-situ experiment required the cathode to be in the form of a pellet so that it could be cycled inside the AMPIX. A series of experiments were performed to identify the optimum ratio of electrode components (6:1:1:2), to ensure good cyclability and conductivity within the AMPIX cell. In particular, both Super P and carbon black were required to obtain electrochemistry that resembled that obtained for electrodes cast on Cu foil (used for the ex-situ studies). The cells were cycled galvanostatically against lithium at constant current at a rate of C/10, between $0.0 – 3.0$ V. Data were collected during the first two discharge/charge cycles.

Pair Distribution Function Analysis. For ex-situ PDF measurements, the electrode materials were scraped off the copper film after cycling and then loaded into kapton capillaries.

X-ray total scattering data were collected at Beamline 11-ID-B of the APS, Argonne National Laboratory. High-energy X-rays (~58keV, λ = 0.2128 Å) were used in combination with a large amorphous-silicon based area detector (Perkin-Elmer) to collect total scattering data to high values of momentum transfer (Q_{max} = ~22 Å). The scattering images were reduced to one-dimensional data using Fit2d.[29] The data were corrected for Compton scattering effects, self absorption, background scattering and detector effects within

PDFgetX2[30] and Fourier transformed to get G(r), the PDF. Structure refinement of the PDF data was carried out using the PDFgui software.[31]

X-ray Absorption Spectroscopy. The XANES measurements were carried out in beamline 9-BM-B/C at the APS, Argonne National Laboratory. In order to minimize absorption effects, both the samples recovered from different states of charge/discharge and the standards were combined with carbon so that the weight percent of the VS_4-rGO/V-standard in the mixture was < 5%. They were then mounted onto a sample holder with a polycarbonate film (< 4 μm thick) and measurements at the S K-edge were recorded in fluorescence yield mode. Energy calibration was done with reference to the lowest energy S K-edge absorption peak of a sodium thiosulfate standard,[32] which was assumed to be at 2469.2 eV. The data was analysed using the Athena software package.[33]

NMR Analysis. ^6Li Magic Angle Spinning (MAS) NMR experiments were performed on VS_4-rGO samples that were cycled with coin cells containing ^6Li enriched lithium metal. The spectra were acquired on a Bruker Avance-300 spectrometer at a ^6Li Larmor frequency of 44.1 MHz. All the experiments were carried out with a Bruker 2.5 mm MAS probe spinning at frequencies of 20 kHz with a rotor synchronised Hahn echo pulse sequence. A 90° pulse of 2.75 μs with a relaxation delay of 10 s was used. ^{51}V MAS NMR experiments were carried out on a Bruker Avance 400 MHz (9.4 T) spectrometer at a ^{51}V Larmor frequency of 105.2MHz with a Bruker 2.5 mm MAS probe spinning at frequencies of 25 kHz. An echo sequence with a $\pi/2$ pulse of 1.5 μs and a recycle delay of 5 s was used. The spectra were referenced to solid NH_4VO_3 at -565.5 ppm.

RESULTS

Crystal structure and DFT studies of VS_4

Figure 1 displays the experimental crystal structure of VS_4, showing linear chains formed along the monoclinic c axis of vanadium atoms in approximately 8-fold coordination of S, with all of the S present as dimerized persulfide S_2^{2-} units. In the experimental structure [Figure 1(a)], the V–V distances along the c direction display an alternation with shorter (2.8 Å) and longer (3.2 Å) distances. By shifting the z coordinate of the V atom to the closest special position, we recover the undistorted structure of VS_4 with equal V–V distances [Figure 1(b)]. DFT calculations suggest that the lower energy, relaxed structure is diamagnetic with a GGA-PBE band gap close to 1 eV, in agreement with the prior work of Rout, C. S. et al[12]. This is seen in Figure 2(a). The use of the HSE functional expands the gap to 1.5 eV for the dimer. The undimerized structure, within DFT, appears to have lost its band gap and displays metallic densities of state, at least in the absence of spin-polarization, and in the absence of any considerations of electron correlation, as seen in Figure 2(b). In order to understand the possible energetics of the true, Peierls distorted state, we have monitored the changes in the energetics upon stepping through the distortion, starting with the undistorted structure. Figure 2(c) displays the DFT energetics, referenced to the ground state of the distorted structure, per 40 atom VS_4 unit cell, as a function of the V–V bond length alternation. The two traces in this panel correpond to static displacements of the V along the c

axis, and displacements accompanied by full structural relaxation (labelled "relaxed"). It is seen that the minimum energy indeed corresponds to a 0.4 Å bond alternation. The depth of the well, close to 0.5 eV per unit cell, would, however, suggest that the undistorted state may be thermally accessible at elevated temperatures.

Electrochemical Characterization

The electrochemical performance of the VS_4-rGO composite was studied by galvanostatic cycling at a rate of C/10 between 3.0 and 0.01 V (Figure 3). The first discharge curve exhibits a flat plateau at 1.9 V (marked 'A'), characteristic of a two-phase reaction. After incorporation of 2.4 Li per formula unit, corresponding to a capacity of ~360 mAh/g, the profile slopes gradually down to 0.01 V. Smaller less distinct processes are observed at ~1.6 V ('B') and 0.7 V ('C'). Although the total discharge capacity in the first cycle is ~2430 mAh/g, the capacity at and below 0.7 V is largely attributed to formation of a solid electrolyte interphase (SEI) arising due to electrolyte decomposition. The capacity down to 0.7 V is ~1200 mAh/g, which agrees with the theoretical capacity corresponding to reaction of VS_4 with 8.0 Li per formula unit to form V metal and Li_2S. Upon charging, the delithiation process is characterized by a rapid rise in potential to 1V and then a more gradual sloping voltage increase to 2.3 V. A noticeable, flatter process is seen at ~2.3 V ('D'), which is similar in length (i.e., capacity) to that seen at ~1.9 V on discharge. The charge capacity is ~1200 mAh/g in the first cycle. The second cycle shows a more sloping profile compared to the first cycle, with a discharge capacity of ~1200 mAh/g that is recovered upon charging. Of note, the 1.9 V process is less distinct on the second discharge, but the process at ~2.3 V is similar to that seen in the 1st cycle.

In-situ X-ray Diffraction

The structural evolution of the pristine material upon galvanostatic cycling was investigated by in-situ X-ray diffraction (SI Figure 1). The capacity obtained from the in-situ cell was ~800 mAh/g in the first discharge. The lower capacity obtained may be related to poor Li ion diffusion through the pellet used as the positive electrode (as opposed to copper film substrate, which was used for the ex-situ coin cells). Only the first two most intense (110 and 020) reflections of the pristine material are clearly visible, and even these are broadened relative to the diffraction pattern obtained ex-situ, due to the high background from the cell components (electrolyte, Li metal, glass fibre separator etc). A continuous decrease, rather than a shift, in the integrated intensity of the 110 and 020 reflections with discharge indicates that VS_4 starts to transform to a more disordered and/or amorphous phase, right from the beginning of discharge. The VS_4 reflections disappear at the end of discharge and do not reappear upon charging. Prior X-ray diffraction of samples prepared ex-situ[11] observed the formation of V metal and Li_2S at the end of discharge; no reflections from any crystalline products at the end of discharge or upon charging the material were seen in this XRD study, possibly because of poorer signal-to-noise and/or smaller particle sizes. We have, therefore, used a range of short range characterization techniques, namely ^6Li and ^{51}V NMR, S K-edge XANES and Pair Distribution Function analysis to probe the nature of the amorphous or nanoparticulate products formed during the charge/discharge process.

NMR. 1st Discharge

[6]Li NMR was carried out on samples stopped at various states of discharge (Figure 4). A resonance at -0.2 ppm is seen upon lithiation to an amount corresponding to 0.66 Li per VS_4 formula unit (denoted as "Li 0.66"), corresponding to a specific capacity of 100 mAh/g. Since the [6]Li/^{7}Li NMR chemical shifts of diamagnetic materials generally lie in the range of 0 ± 3 ppm, the resonance at Li 0.66 is therefore attributed to a diamagnetic intermediate, tentatively assigned at this point to V in a higher oxidation state (+5). As lithiation progresses, this resonance shifts to slightly higher frequency (~0.5 ppm). Upon further lithiation, at Li 2.0 (i.e., at the end of process A), a broad resonance close to ~25 ppm is observed. In general, such a broad and shifted resonance is due to hyperfine interactions arising due to lithium ions being close to paramagnetic ions,[34] and is therefore indicative of formation of reduced V^{4+} species at this stage of the discharge process. This broad feature becomes broader on further discharge, remains until Li 3.4, and then disappears into the baseline. The growth of a peak at 2.2 ppm due to Li_2S formation also starts to become evident at this stage (Li 2.0) with this resonance becoming more prominent and growing in intensity upon further lithiation (between Li 2.67 – Li 8.0). The resonance seen at ~0 ppm towards the end of discharge is attributed to be due to diamagnetic components such as LiOH, Li_2CO_3 and other lithium salts arising from SEI formation at low voltages[35] on both VS_4 and the various carbons (including graphene oxide) used to fabricate the electrode. The integrated intensity of this peak increases in intensity with discharge until Li 2.0 (see plot in supplemental figure, SI.2) then decreases in intensity from Li 2.0 to Li 2.67. This is followed by a continuous growth in the intensity of this peak from Li 2.67 to Li 8.0. Therefore, in the initial stages of the discharge profile, this peak is attributed to the diamagnetic V^{5+}-containing intermediate, but beyond Li 2.66, the increase in intensity is ascribed at least in part to the growth of a second overlapping peak from the diamagnetic species that form part of the SEI as discharge progresses down to 0 V (SI. 2).

The local structure of vanadium compounds can also be probed by using [51]V NMR spectroscopy. The starting material, VS_4, which has V in +4 oxidation state, might be expected to be paramagnetic, and thus would not be expected to give readily detectable high resolution NMR spectrum owing to the extreme line broadening resulting from fast relaxation of the metal nuclei and the large hyperfine shifts. The observation of a [51]V NMR spectrum for the pristine material (Figure 5), with an isotropic shift of ~161 ppm, suggests, however, that it is actually diamagnetic. Spin-pairing in this material must arise due to the Peierls distortion described previously and observed in the DFT calculations, which leads to the observed alternation in V-V distances (3.2 Å and 2.8 Å)[13] as well as the nearly 1 eV semiconducting gap in the density of states. Simulations of the [51]V spectrum (see SI. 3) yielded a large chemical shift anisotropy (δ(CSA) = -1520 ppm, asymmetry parameter, η(CSA) = 0.6) and a moderate quadrupolar coupling constant, C_Q of 134 kHz, (η(Quad) = 0.4). While the C_Q determination (and the values of the CSA and C_Q asymmetry parameters) is less reliable due to the difficulty in exciting the whole spectrum, the large CSA is noteworthy, its large value being ascribed to the anisotropy in V bonding (due to the formation of V-V bonds).

The ^{51}V NMR of discharged samples was carried out at two different field strengths, 9.4 and 16.4 T. The ^{51}V NMR of samples measured at 9.4 T are given in Figure 5. Upon lithiation to Li 0.66, in addition to the broad resonance characteristic of the pristine sample, an additional site characterized by an isotropic shift at ~1430 ppm is observed. This chemical shift is found to be close to that of a model compound, K_3VS_4 (1375 ppm), which is comprised of diamagnetic V(V) ions bound to S^{2-} sulphur ligands to form isolated tetrahedral units (SI.4). The analogous material, Li_3VS_4, has not been synthesized, however, the dimethyl formamide adduct phase $Li_3VS_4.2DMF$ has been prepared.[36] The solution ^{51}V NMR of this compound in Me_2SO exhibits a ^{51}V NMR shift of 1388 ppm.[37] The NMR shifts of the tetrathiovanadate ion (VS_4^{3-}) in a range of other solvents are in the range of 1395-1400 ppm.[35-37] All this data suggests that the resonance at ~1430 ppm is due to a material with composition close to Li_3VS_4, a material in which the S_2^{2-} sulfur ions have been reduced to S^{2-}, while the vanadium ions have been oxidized to V^{5+}, in agreement with the ^{6}Li NMR spectrum of this material. Upon further lithiation to a specific capacity of 300 mAh/g (Li 2.0; end of process A), the peak at 1430 ppm diminishes and a new environment characterized by an isotropic shift at ~-546 ppm is observed (Figure 5, SI. 5). In general, the vanadium nucleus is more deshielded as the polarizability of the ligand increases and vanadium compounds with sulphur ligands generally have higher frequency shifts compared to those with oxide ligands.[37-39] ^{51}V shifts of ~-550 ppm are not therefore characteristic of V(V) sulphides and are more commonly exhibited by the vanadium oxides (vanadates).[40, 41] However, it has been observed that reduction of V(V) to form mixed valent V(IV)/ V(V) vanadium oxides can result in large negative shifts from ~-550 ppm to ~-1440 ppm.[41] Thus, the negative shift from ~1440 ppm to -547 ppm is similarly ascribed to partial reduction of V(V) to V(IV) as the discharge progresses. The huge shift in the ^{51}V NMR from ~1440 ppm to ~ -550 ppm is attributed to the hyperfine interaction of V^{5+} ions with nearby V^{4+} ions (in the 1st V^{5+} cation coordination shell) in the mixed valent compound formed at this stage. Note that the V^{4+} ions are not likely to be observed under the conditions used to acquire these spectra. The ^{6}Li NMR spectrum for Li = 2.0 exhibits a broad feature at ~25 ppm further supporting the formation of a paramagnetic material comprised of both V(IV) and V(V). Beyond this, at Li 2.68, a resonance at 5657 ppm is observed. The ^{51}V NMR spectrum of the body centered cubic (bcc) form of elemental V (the thermodynamic phase[42]) exhibits a shift of ~5230 ppm (SI. 6). The shift at 5657 ppm is also attributed to V metal, the discrepancy being attributed to the formation of the face centered cubic (fcc) polymorph V upon discharge. This is supported by the PDF data shown in the following section. The spectra obtained at a field strength of 16.4 T concur with the above results (SI. 7). However, resonances due to V metal are observed (SI. 8) in this set of samples right from the beginning of discharge possibly due to instability of some of the products and disproportionation leading to metal deposition.

NMR. 1st Charge.

The ^{6}Li NMR resonances at 2.2 ppm and ~0.5 ppm, from Li_2S and SEI components, respectively, remain on charging to 0.5 V (Figure 6). The Li resonance from the SEI is a superposition of several Li environments resonating between -1 ppm (LiF) and +1 ppm (LiOH). Thus, the small variations in shift in the resonance from 0 ppm (at the end of

discharge) to ~0.5 ppm on charging to 0.5 V and then ~0 ppm, as charging progresses further, are ascribed to slight variations in the SEI composition between the different samples. At 2.3 V, ie., at the end process D, a broad resonance at ~ 8 ppm is observed along with a slight decrease in the Li_2S resonance. This is attributed to the partial reformation of the Li_{3+x},VS_4 intermediate, the different shift from that observed on discharge indicating a slightly different Li content and vanadium oxidation state. The peak at ~2.2 ppm decreases in intensity as charging progresses and disappears at 3 V indicating that Li_2S further converts to another phase as charging progresses.

On charging to 2.3 V, i.e., at the end of process D, a ^{51}V NMR resonance is seen at -568 ppm (Figure 7). The lineshape of this resonance differs noticeably from that of the pristine material in that it has a sharp central transition, with a broad spinning sideband manifold from the satellite transitions. The chemical shift anistropy is noticeably smaller for the -568 ppm resonance indicating that it arises from a more symmetric local environment. The extraction of NMR parameters, which would give further insights into the causes of the broadening of these spectra requires excitation of the entire spinning sideband manifold at two different field strengths, which was not possible under the present experimental conditions. The shift (and sideband manifold) of this resonance is close to that of the $Li_{3+x}VS_4$ resonance observed during the discharge process (see Figure SI. 5) suggesting that a structurally related intermediate is formed during charging, however, with a slightly different Li content and vanadium oxidation state. This proposal is consistent with the ^6Li NMR spectra. The intensity of this resonance increases on charging up to 3 V. A broad intense hump is observed under the main (sharp) resonance, which is more prominent in the 3V sample. This is ascribed to amorphous VS_4, the broadening arising either from electron-nuclear dipolar coupling due to paramagnetic V^{4+} ions caused by non-stoichiometry, or regions of the sample that do not undergo a Peierls distortion, and/or simply a distribution of local environments in the disordered material.

S K-edge XANES Spectroscopy.

S K-edge XANES was carried out in order to investigate the evolution of the oxidation states of S as a function of state of charge/discharge. Figure 8 and Figure SI. 9 show the normalized absorption spectra and first derivative of the normalized absorption spectra, respectively, of the lithiated VS_4 phases and a series of S-containing model compounds. S K-edge XANES of transition metal sulphides are particularly useful as the relative shifts and intensities of the pre-edge peak are sensitive to the covalency of the metal-ligand bond, yielding information on not just the oxidation state of the S but also of the transition metal ion. The pre-edge features in the S K-edge spectra arise from excitation of electrons from the S 1*s* orbitals to S3*p*/V3*d* antibonding states.[43, 44] The higher the positive charge on the metal, the more stabilized the hybridized S 3p orbitals are. As a result, the pre-edge peaks shift to lower energies with increasing effective positive charge on the metal. The S K-edge spectra of the model compounds demonstrate this trend with K_3VS_4 (V(V)) and $LiVS_2$ (V(IV)) (both containing S^{2-}) exhibiting pre-edge peaks at 2466.8 eV and 2467.2 eV, respectively. Changes in S oxidation state and ionicity produce more noticeable changes: VS_4 with S_2^{2-} (-1 formal oxidation state) dimers will have a lower energy 1 s orbital as compared to S^{2-} leading to a

higher energy pre-edge peak at 2469.0 eV. S exhibits a peak at still higher energies at 2469.8 eV. Li_2S in which there is no significant covalent interaction with metal centers has no pre-edge features and exhibits characteristic absorption peaks at 2475.7 eV and 2478.4 eV. The experimentally observed absorption profile of Li_2S (Figure 8) also contains features at 2469.8 eV similar to that in S which may be attributed to some decomposition of Li_2S to S, possibly due to slight air exposure before taking the measurements.

The shifts of the model compounds can be used as a fingerprint to assign the oxidation state of S in the cycled samples. The XANES spectrum of the sample discharged to Li 0.66 exhibits peaks at 2469.0 eV and 2466.9 eV corresponding to VS_4 and an intermediate with a structure similar to that of K_3VS_4 (possibly Li_3VS_4), respectively. At Li 2.68, the peak at 2469.0 eV has disappeared and only the peak at 2466.9 eV remains. At the end of discharge, characteristic features in the absorption spectra due to Li_2S are observed. On charging, the absorption profile at 2.3V is similar to that of K_3VS_4 suggesting that the charging process occurs through reformation of the same Li_3VS_4-like intermediate. At the end of charge, the absorption profile exhibits a peak at 2469.0 eV characteristic of VS_4 suggesting partial reformation to a phase that is similar to VS_4 upon charging and that, significantly, contains S_2^{2-} ions.

Pair Distribution Function Analysis.

PDFs obtained from X-ray total scattering data have proven to be an invaluable tool to investigate the structures of x-ray amorphous/nanoparticulate intermediates formed during the cycling of Li-ion batteries.[45,46, 47, 48] Figure 9 shows the ex-situ PDF patterns obtained in the first discharge cycle. The PDF pattern at Li = 0.0 corresponds to that of VS_4. Correlations due to S-S dimers of VS_4 are seen at 2.0 Å (marked 'I') while the correlations at 3.2 Å correspond to the V-V distance in VS_4 ('III'). Within the unit cell, the ratio of V-V distances at 3.2 and 2.8 Å is 2:1, and thus the latter distance therefore appears only as a very small peak in even the simulated PDF and is hardly visible in the experimental PDF of the pristine material. However the presence of the correlation at 3.2 Å is evidence of the distortion in the V-V distances in the material. The correlation at 2.4 Å ('II') corresponds to the V-S distance in VS_4 but this overlaps with correlations due to bond distances in fcc V metal (2.6 Å) and Li_2S (2.5 Å). Up to Li 2.0 (till the end of process 'A'), the correlations beyond 4.0 Å are quite broad, suggesting a range of bond distances characteristic of a highly amorphous intermediate formed at this stage. From Li 2.68 (from process 'B') down to 0V , sharper more well defined correlations due to fcc V are seen. A PDF refinement of the product formed at the end of discharge confirms that the phase formed at the end of discharge is the metastable phase fcc V (particle size of ~6.5 nm, SI. 10). These correlations weaken upon charging and reappear again upon discharge in the second cycle. The changes seen in the PDF patterns are clearer in the difference PDF patterns in which each PDF pattern is subtracted from the one prior to it in the discharge curve (Figure 10). A negative correlation in the difference PDF is suggestive of the particular bond being broken or a correlation disappearing while a positive correlation indicates that a bond (correlation) is being formed. As discharge progresses, the negative correlation marked 'A' in the inset corresponds to the

breaking of the S-S dimers at 2.0 Å. This is accompanied by a positive correlation at 2.2 Å (marked 'B'). This is attributed to the V-S bond in the tetrahedral VS_4 units of the Li_3VS_4 species formed at this stage. This bond then breaks leading to formation of V metal as shown in the inset. Although correlations due to VS_4 at the end of charge are not sharp, negative correlations due to fcc V upon charging indicate unambiguously that the V metal is consumed as charging progresses. This demonstrates that reversibility in this system is not solely due to Li_2S reacting to form S as has been suggested previously,[11] but involves reaction of V metal and at least partial conversion back to a phase structurally related to VS_4. A Principal Component Analysis (PCA) performed on the entire dataset of the PDF data[49] provided further confirmation of the multiple phases formed during the charge-discharge process. It was found that three eigenvectors were required to explain 98 % of the variance in the experimental data while a fourth eigenvector adds only a marginal improvement and is attributed to noise, and therefore the analysis yields three principal components (SI. 11). The first two components are dominated by contributions from fcc V and VS_4, respectively, and the third component is attributed to formation of intermediate phases. The PCA is not sensitive to the small changes in lithium content in $Li_{3+x}VS_4$ identified by NMR spectroscopy. The analysis indicate the growth of the intermediate phase upto Li 2.0 followed by formation of fcc V metal which grows till the end of discharge consistent with the NMR and PDF data (SI. 12).

DISCUSSION

VS_4 has a structure comprised of V^{4+} ions coordinated to four sets of sulphur dimers to form linear chains along the c-axis. The results presented here (in particular the ^{51}V NMR spectrum) provide clear evidence for the electronic structure of this material (which has prior to this not been clearly described), namely that it contains paired electrons (in V-V bonds) as opposed to the unpaired electrons typically observed in V^{4+} ions. This is consistent with DFT calculations of the densities of states of VS_4 as well as studies of the energy stabilization obtained by going from an undistorted, paramagnetic and metallic state to the actual distorted/dimerized state The metal-metal distances seen in VS_4 are consistent with those seen in other Peierls distorted compounds such as β-VO_2.[50] The large ^{51}V CSA is ascribed to the anisotropy in V bonding (due to the formation of V-V bonds) as is observed in β-VO_2, which exhibits a shift anisotropy of ~1159 ppm. Peierls distortions are frequently observed in a range of other 1-dimensional and 2-dimensional transition metal compounds, such as $NbSe_3$ and TaS_3, materials in which the transition metal ion has partially filled d-levels, and where a dimerization serves to lift the degeneracy at the Fermi level and lower the electronic energy of the system as a whole.[51] Metal-insulator transitions are characteristic of Peierls distorted compounds and further studies are underway to study this phenomenon in this material.

VS_4 undergoes a complex series of redox reactions on lithiation. Initially the sulphur dimers in VS_4 are broken and the VS_4 is converted to a phase with a stochiometry close to Li_3VS_4 (analogous to K_3VS_4) in the plateau region (A). This process involves an unusual internal redox reaction whereby one electron from V^{4+} is transferred to S_2^{2-} dimers (along with 3 e$^-$ from the external circuit), the V^{4+} being oxidized to V^{5+} and S_2^{2-} being completely

reduced to S^{2-} resulting in the formation of Li_3VS_4. Consistent with this, the phase that is formed is diamagnetic, giving rise to a characteristic diamagnetic signal in the ^6Li NMR spectrum (at ~ 0 ppm) and a ^{51}V resonance at ~1430 ppm. The intensity of the ^{51}V resonance is, however, quite low and it is likely a result of a relatively long spin-lattice (T_1) relaxation process for ^{51}V in the tetrahedral environment, the signal not being fully recovered in the 5 s relaxation delay used in the NMR experiments. This proposal is supported by our measurements of the analogous compound K_3VS_4, which had a T_1 time of greater than 25 s.

In order to explore the energetics of this process, we compared the band structures of VS_4 with that of Li_3VS_4 (Figure SI. 13) by performing calculations using the structure of K_3VS_4, replacing K^+ by Li^+ (and performing geometry optimizations). The results indicate stabilization of the Fermi energy upon formation of the lithiated intermediate Li_3VS_4, giving further evidence that such an internal redox process is energetically favorable. (We note that we are unlikely to have found the ground state Li_3VS_4 structure; the relative lowering of the Fermi energy for this structure is likely to be even more pronounced). Such an internal redox process has been observed to occur chemically in vanadium-thiol complexes which contain patronite-like $V_2(S_2)_2$ units.[52] Reaction of a VS_4^{3-} solution with tetraisobutylthiuram disulphide results in the formation of a novel vanadium (IV) dimer ($V^{IV}_2(S_2)_2(i\text{-}Bu_2NCS_2)_4$) formed by an induced internal reaction whereby reduction of V^{5+} is accompanied by oxidation of S^{2-}. The latter complex has a $V_2(S_2)_2$ structural unit similar to that seen in patronite with a V-V bond having a distance of 2.8 Å. This sort of internal electron transfer is facilitated by hybridization of metal d bands with bands belonging to the ligand (in this case S_2^{2-}) although further band structure calculations of VS_4 are needed to confirm this.

Once full reduction to sulfide has occurred, further lithiation occurs which involves reduction of V^{5+} to V^{4+} as indicated by the appearance of a paramagnetic feature in the ^6Li NMR spectrum at this stage of the discharge profile. However the observation of a ^{51}V NMR signal suggests that the intermediate formed at this stage also has some vanadium diamagnetic centers and the shifted ^{51}V resonance (at -546 ppm) is attributed to a mixed valent compound with both V(IV) and V(V) centers, V(V) centers giving rise to the -546 ppm resonance. Further reduction leads to the formation of fcc V and Li_2S. These redox processes are summarized in Figure 11. In contrast to the oxides where redox activity is primarily centered on the transition metal ion, in the sulphides it is observed that extensive covalency of the metal-ligand bond causes redox activity to involve the ligand as well. This has been seen earlier in the thiospinels[53] for instance, where an interplay between S^{2-} and S_2^{2-}, attributed to hybridization of metal-sulfur orbitals, is observed. The present is a unique case among the sulphides involving oxidation of the cation concomitant with reduction of the anion. A similar chemistry has been proposed with regard to the the Li-rich oxides ($Li_2Ru_{1-y}Sn_yO_3$) where reduction of Ru^{6+} to Ru^{5+} is accompanied by oxidation of O^{2-} to O_2^{2-}.[54]

V metal is in general stable as the bcc polymorph.[42] However, previous studies of V nanoparticles formed during ball-millling of V metal in a nitrogen atmosphere have observed the formation of fcc V, which is formed along with the formation of δ-VN.[55] The V metal formed towards the end of the discharge cycle is similarly nanoparticulate and presumably

forms with a large number of defects, the former leading to a large surface to volume ratio. Presumably, the fcc form minimizes the surface energies,[55] which is possibly further facilitated by the occlusion of C atoms into the structure from the electrolyte.

Upon charging, the resonance at ~-565 ppm is indicative of the formation of the lithiated intermediate whose composition is tentatively assumed to be $Li_{3.5}VS_4$. . Delithiation to form $Li_{3.5}VS_4$ would yield a charge capacity of ~525 mAh/g. However the capacity observed upon charge is in excess of this, suggesting that further delithiation to form VS_4 also occurs. The S K-edge XANES spectra at the end of charge (3V) indicates that a phase similar to VS_4 is formed. This phase is clearly amorphous/disordered as no reflections are observed in the diffraction pattern. However, the PDF pattern clearly shows evidence for both S_2^{2-} ions and V-S bonds The ^{51}V NMR signal at 161 ppm characteristic of VS_4 is not however observed upon charging, however a very broad signal around this chemical shift range is observed (in addition to the ~-565 ppm resonance. This discrepancy can be a consequence of the greater degree of disorder of the VS_4 phase formed upon charging. As a result, defects are likely present so that complete spin pairing of all the adjacent V atoms does not occur leading to the presence of paramagnetic centers and peak broadening.

Reversibility in Li ion batteries is generally contingent upon there being minimal structural reorganization during charging and discharging of the battery. In conversion electrode materials however there is no topochemical structural relationship between the starting material and the product obtained at the end of discharge and extensive bond breaking occurs during the redox process. The large activation energy required for reformation of the starting material contributes to the large voltage hysteresis between discharge and charge cycles. With increasing covalency of the M-X bond, this voltage gap decreases, with fluorides generally exhibiting a larger voltage gap between discharge and charge when compared with sulphides and phosphides.[6, 47] The reaction to form V + Li_2S studied here exhibits a ΔE_{hys} of 1.0 -1.3 V (Figure SI. 14), which is comparable to that of many other sulfide conversion materials. However, as appears increasingly to be the case for many of these systems,[56] the difference between the structural pathways taken on discharge and charge must also contribute to the hysteresis. The good reversibility in this system is partly attributed to the rGO which forms a conducting pathway over the insulating products formed at the end of discharge.

CONCLUSIONS

In conclusion, we have used a range of short range characterization techniques (NMR, PDF and XANES) to elucidate the structural transformations occurring during complete reductive lithiation (addition of 8 Li per formula unit) of the Peierls distorted vanadium sulphide, VS_4. The studies are complemented by an examination of the DFT electronic structure of VS_4. Unlike many of the electrode materials where electron transfer is centered either on the cation or on the anion, here we observe a complex redox interplay involving electron transfer between the cation and the anion leading to the breaking of the S-S dimers of VS_4 and the formation of metastable intermediates such as Li_3VS_4. This process is found to be partially reversible and is here attributed to extensive metal-ligand covalency in VS_4.

ACKNOWLEDGEMENTS

Supporting Information Available:

In-situ X-ray Diffraction data, additional ^{51}V NMR data, first derivative of the normalized S K-edge XANES spectra as well as absolute DOS of VS_4 and Li_3VS_4 are provided as Supporting Information. This information is available free of charge via the internet at http://pubs.acs.org.
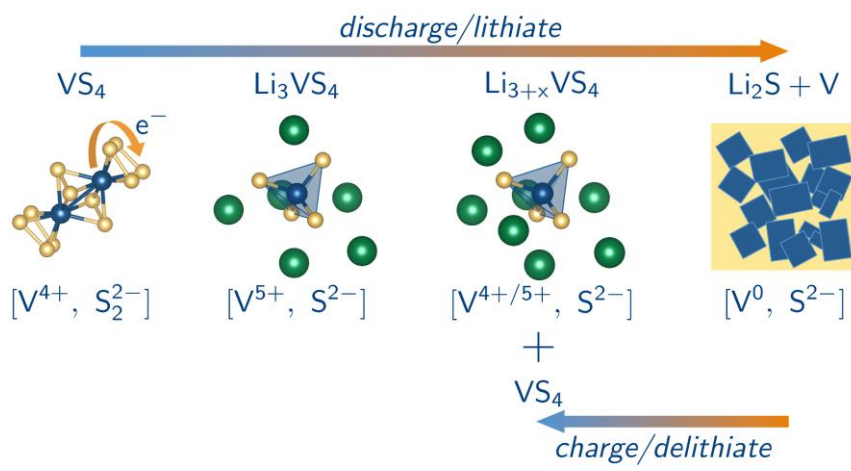
REFERENCES

(1) Mizushima, K., Jones, P. C., Wiseman. P. J., Goodenough, J. B. *Mater. Res. Bull.* **1980**, *15*, 783–789.

(2) Dahn, J. R.; Zheng, T.; Liu, Y.; Xue, J. S. *Science* **1995**, *270*, 590–593.

(3) Kim, Y.; Arumugam, N.; Goodenough, J. B. *Chem. Mater.* **2008**, *2*, 470–474.

(4) Masquelier, C.; Padhi, A. K.; Nanjundaswamy, K. S.; Goodenough, J. B. *J. Solid State Chem.* **1998**, *135*, 228–234.

(5) Padhi, A.; Nanjundaswamy, K. *J. Electrochem. Soc.* **1997**, *144*, 2581–2586.

(6) Cabana, J.; Monconduit, L.; Larcher, D.; Palacin, R. M. *Adv. Mater.* **2010**, *22*, E170–E192.

(7) Whittingham, M. *Prog. Solid State Chem.* **1978**, *12*, 41–99.

(8) Debart, A.; Dupont, L.; Patrice, R.; Tarascon, J.-M. *Solid State Sci.* **2006**, *8*, 640–651.

(9) Golodnitsky, D.; Peled, E. *Electrochim. Acta.* **1999**, *45*, 335.

(10) Hillebrand, W. F. *J. Am. Chem. Soc.* **1907**, 1019–1029.

(11)   Xu, X.; Jeong, S.; Rout, C. S.; Oh, P.; Ko, M.; Kim, H.; Kim, M. G.; Cao, R.; Shin, H. S.; Cho, J. *J. Mater. Chem. A* **2014**, *2*, 10847–10853.

(12)   Rout, C. S.; Xu, X.; Yang, J.; Jeong, H. Y.; Odkhuu, D.; Park, N.; Cho, J.; Shin, H. S. *J. Am. Chem. Soc.* **2013**, *135*, 8720–8725.

(13)   Allmann, R.; Baumann, I.; Kutoglu, A.; Rosch, H.; Hellner, E. *Naturwissenschaften* **1964**, *51*, 263

(14)   Whangbo M, H and Gressier, P. *Inorg. Chem.* **1984**, *23*, 1228-1232

(15)   Klemm, W.; Schnering, H. G. *Naturwiss*. **1965**, *52*, 12.

(16)   Klemm, W.; Hoschek, E. *Z. Anorg.u. Allgem. Chem.* **1936**, *226*, 359

(17)   Lapina, O. B.; Khabibulin, D. F.; Shubin, A. A.; Terskikh, V. V. *Prog. Nucl. Magn. Res. Spec.* **2008**, *53*, 128.

(18)   Kresse, G and Hafner, J. *Phys. Rev. B* **1993,** *47***,** 558-561

(19)   Kresse, G and Hafner, J. *Phys. Rev. B.* **1994**, *49,* 14251-14269

(20)   Kresse, G and Furthmuller, *J. Comput. Mat. Sci.* **1996**, *6***,** 15-50

(21)   Kresse G and Furthmuller, *J Phys. Rev. B.* **1996**, *54***,** 11169

(22) Blöch P. E Phys. Rev. B. **1994**, *50***,** 17953

(23) Kresse, G and Joubert, D Phys. Rev. B. 1999, *59***,** 1758

(24) Perdew J. P, Burke, K and Ernzerhof, M. Phys. Rev. Lett. **1996**, *77***,** 3865

(25)   Heyd, J.; Scuseria, G. E.; Ernzerhof, M. *J. Chem. Phys.* **2006**, *124,* 219906.

(26)   Momma, K.; Izumi F, *J. Appl. Crystallogr.* **2011**, *44*, 1272-1276.

(27)   Kovtyukhova, N. I.; Ollivier, P. J.; Martin, B. R.; Mallouk, T. E.; Chizhik, S. A.; Buzaneva, E. V. Gorchinskiy, A. D. *Chem. Mater.* **1999**, *11*, 771

(28)   Borkiewicz, O. J.; Shyam, B.; Wiaderek, K. M.; Kurtz, C.; Chupas, P. J.; Chapman, K. W. *J. Appl. Cryst.* **2012**, *45*, 1261-69

(29)   Hammersley, A., **1998,** *FIT2D V9.129 reference manual V3.1. ESRF internal report 98HA01T, ESRF.*

(30)   Qiu, X.; Thompson, J. W.; Billinge, S. L. J. *Appl. Cryst.* **2004,** *37*, 678.

(31)   Farrow, C. L.; Juhas, P.; Lui, J. W.; Bryndin, E. S.; Bozin, J.; Bloch, T.; Proffen, T.; Billinge, S. J. L., *Journal of Physics: Condensed Matter* **2007,** *19*, 335219.

(32)   Sekiyama, H.; Kosugi, N.; Kuroda, H.; Ohta, T. *Bull. Chem. Soc. Jpn*. **1986**, *59*, 575

(33)   Ravel, B.; Newville, M. *J. Synchrotron. Radiation* **2005**, *12*, 537

(34)   Grey, C. P.; Dupré, N. *Chem. Rev.* **2004**, *104*, 4493.

(35)   Meyer, B. M.; Leifer, N.; Sakamoto, S.; Greenbaum, S. G.; Grey, C. P. *Electrochem. Solid State Lett.* **2005**, *8*, A145.

(36)   Zhang, Y. P.; Holm, R. H. *Inorg. Chem.* **1988**, *27*, 3875

(37)   Hayden, Y. T.; Edwards, J. O. *Inorganica Chim. Acta* **1986**, *114*, 63–69.

(38)   Harrison, A. T.; Howarth, O. W. *J. Chem. Soc. Dalton Trans.* **1986**, 1405.

(39)   Simonnet-Jégat, C.; Sécheresse, F. *Chem. Rev.* **2001**, *101*, 2601–2612.

(40)   Rehder, D.; Weidermann, C.; Duch, A.; Priebsch, W. *Inorg. Chem.* **1988**, *27*, 584-587

(41)   Delmaire, F.; Rigole, M.; Zhilinskaya, E. A.; Aboukais, A.; Hubaut, R.; Mairesse, G. *Phys. Chem. Chem. Phys.* **2000**, *2*, 4477-4483

(42)   Carlson, O. N.; Owen, C. V. *J. Electrochem. Soc.* 1960, 107, 69.

(43)   Fleet, M. E.; Liu, X.; Harmer, S. L.; King, P. L. *Can. Mineral.* **2005**, *43*, 1605-1618

(44)   Solomon, E. I.; Hedman, B.; Hodgson, K. O.; Dey, A.; Szilagyi, R. K. *Coordn. Chem. Rev.* **2005**, *249*, 97

(45)   Yamakawa, N.; Jiang, M.; Key, B.; Grey, C.P. *J. Am. Chem. Soc.* **2009**, *131*, 10525

(46)   Dambournet, D.; Chapman, K. W.; Chupas, P. J.; Gerald, R. E.; Penin, N.; Labrugere,C.; Demourgues, A.; Tressaud, A.; Amine, K. *J. Am. Chem. Soc.* **2011**, *133*, 13240.

(47)   Hua, X; Robert, R.; Du, L.-S; Wiaderek, K. M.; Leskes, M.; Chapman, K. W.; Chupas, P. J.; Grey, C. P. *J. Phys. Chem. C.* **2014**, *118*, 15169.

(48)   Shyam, B.; Chapman, K. W.; Balasubramanian, M.; Klingler, R. J.; Srajer, G.; Chupas, P. J. *Angew. Chem. Int. Ed. Engl*. **2012**, *51*, 4852.

(49)   Chapman, K. W.; Lapidus, S.; Chupas, P. J. "Applications of Principal Component Analysis to Pair Distribution Function Data", *J. Appl. Cryst.,* submitted.

(50)   Nielsen, U. G.; Skibsted, J.; Jakobsen, H. J. *Chem. Phys. Lett.* **2002**, *356*, 73.

(51)   Smaalen, S. *Acta Cryst. A.* **2005**, *A61*, 51.

(52) Halbert, T. R.; Hutchings, L. L.; Rhodes, R.; Steifel, E. I. *J. Amer. Chem. Soc.* **1986**, *108*, 6437-6438

(53)   Bodenez, V.; Dupont, L.; Morcrette, M.; Surcin, C.; Murphy, D. W.; Tarascon, J. -M. *Chem. Mater.* **2006**, *18*, 4278

(54)   Sathiya, M.; Rousse, G.; Ramesha, K.; Laisa, C. P.; Vezin, H.; Sougrati, M. T.; Doublet, M.-L.; Foix, D.; Gonbeau, D.; Walker, W.; Prakash, A. S.; Hassine, M. B.; Dupont,   L.; Tarascon, J.-M. *Nature Materials*, **2013**, *12*, 827.

(55) Lopez-Flores, V.; Roldan, M. A.; Real, C.; Paez, A. M.; Castro, G. R. *J. Appl. Phys.* **2008**, *104*, 023519.

(56) Yu, H-C.; Ling, C.; Bhattacharya, J.; Thomas, J. C.; Thornton, K.; Van der Ven, A.; *Energy Environ. Sci.* **2014**, 7, 1760.

Table of Contents Figure

discharge/lithiate

VS_4 Li_3VS_4 $Li_{3+x}VS_4$ $Li_2S + V$

$[V^{4+}, S_2^{2-}]$ $[V^{5+}, S^{2-}]$ $[V^{4+/5+}, S^{2-}]$ $[V^0, S^{2-}]$

$+$

VS_4

charge/delithiate
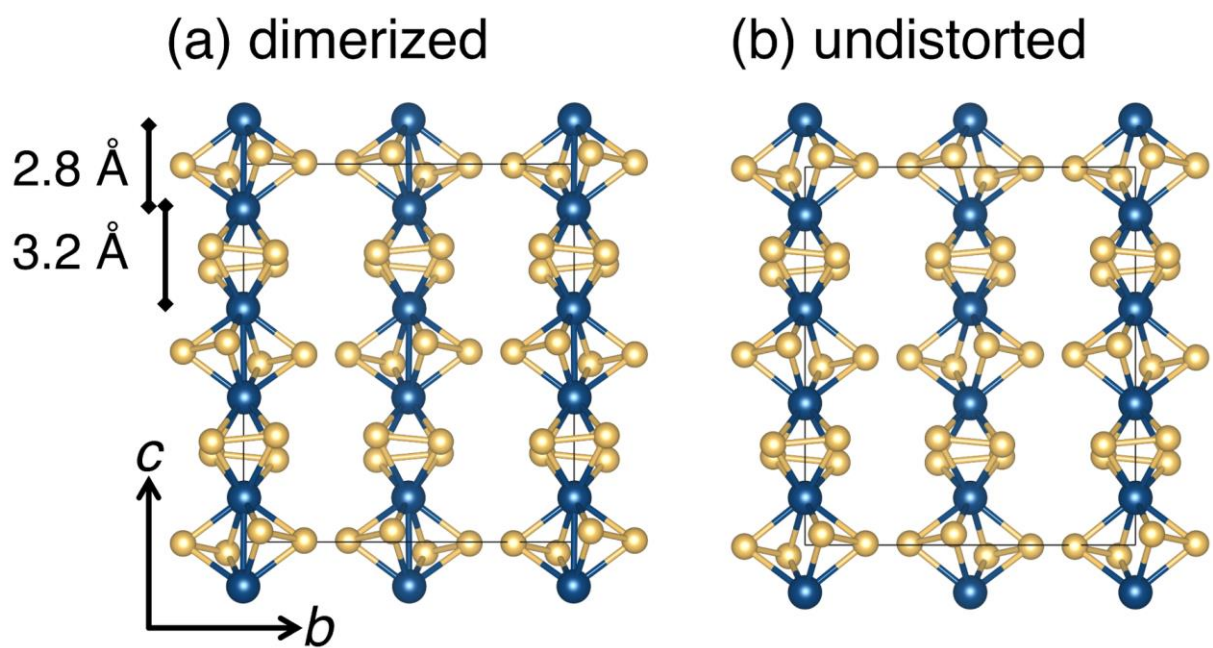
Figures

Figure 1. Structure of (a) dimerized, Peierls distorted VS_4 and (b) an undistorted version, projected down the *a* axis.
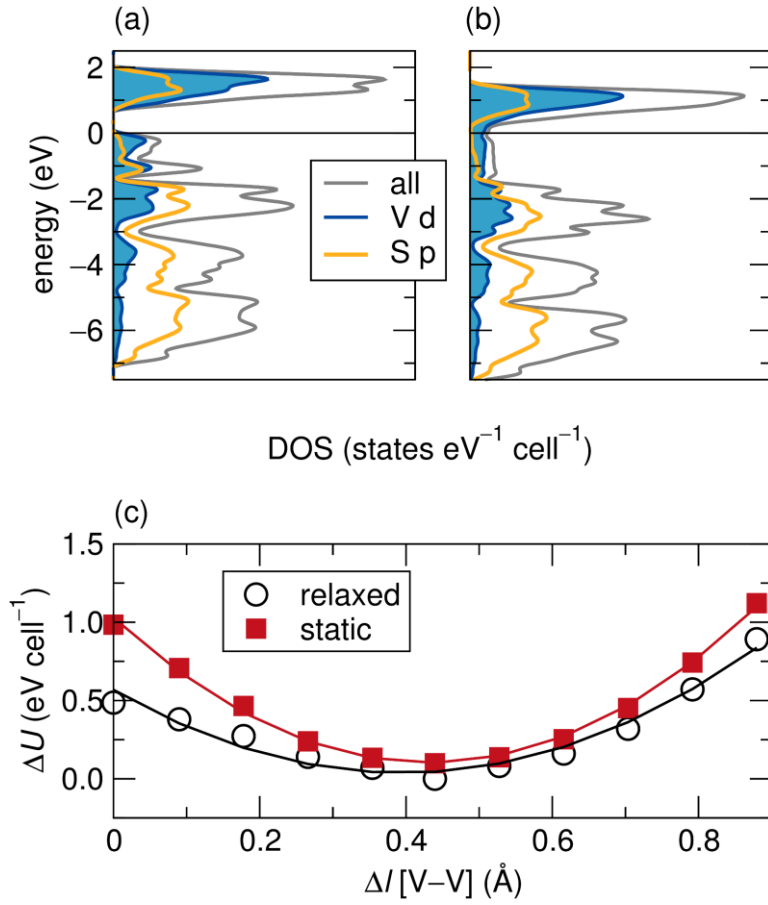
Figure 2. Densities of states (DOS) for (a) Peierls-distorted VS$_4$ and (b) its undistorted variant, showing that the distortion opens an insulating gap in the densities of state. (c) Energetic stabilization per unit cell arising from the Peierls distortion, depicted as a function of the bond alternation, the difference in length between the short and long V−V distances along the *c* direction.
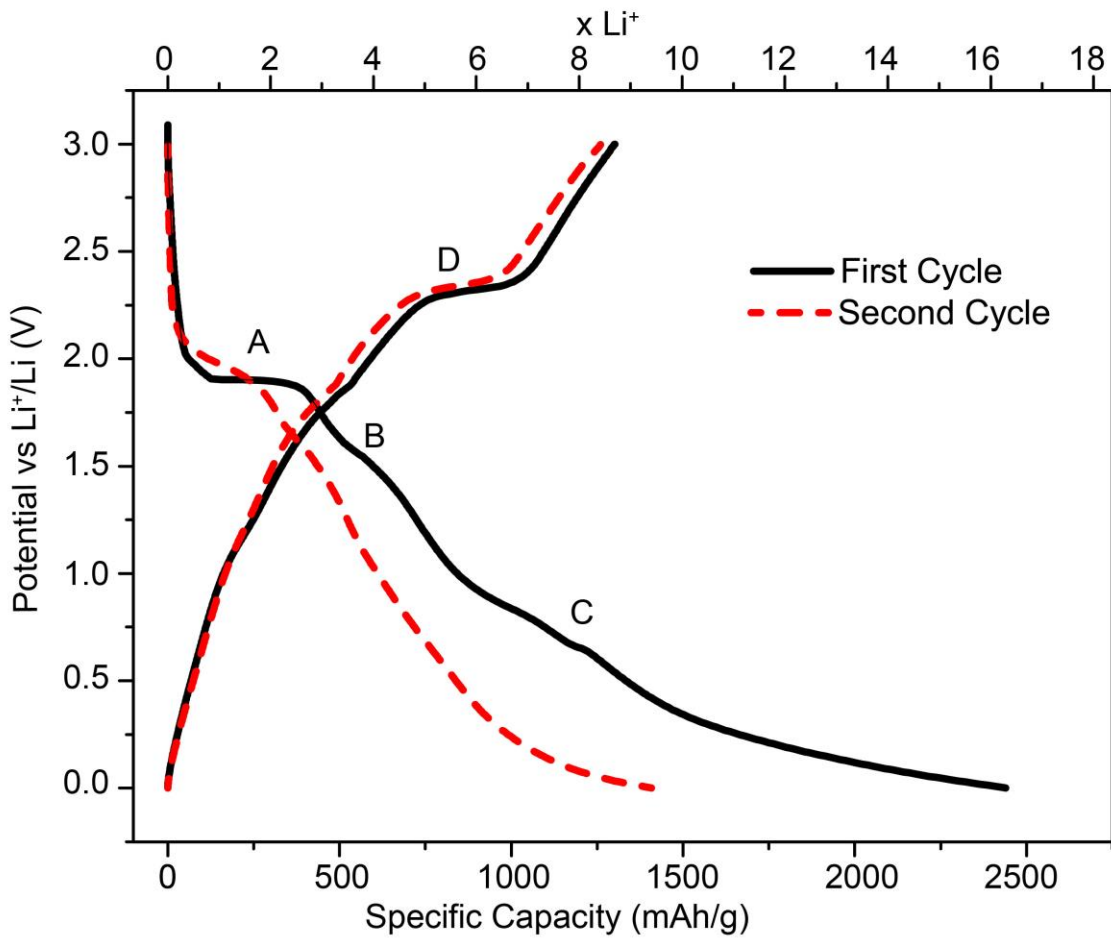
Figure 3. Galvanostatic charge-discharge curve of VS$_4$-rGO cycled between 0.0 and 3.0 V at a rate of C/10. The first two cycles are shown. A, B, C and D correspond to the more pronounced processes that are described in the text.
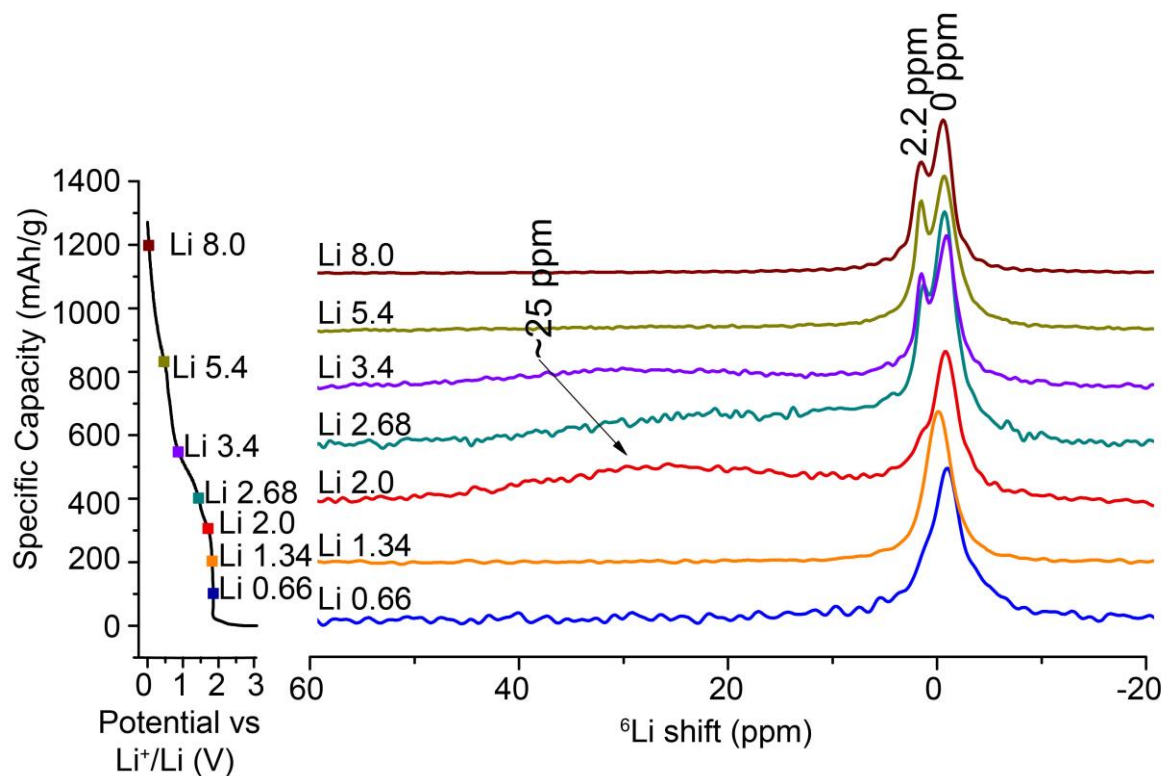
Figure 4. ^{6}Li MAS NMR spectra of discharged VS$_4$-rGO samples between Li = 0.66 – 8.0, acquired at a field strength of 7.05 T. The intensities were normalized with number of scans and weight of sample.
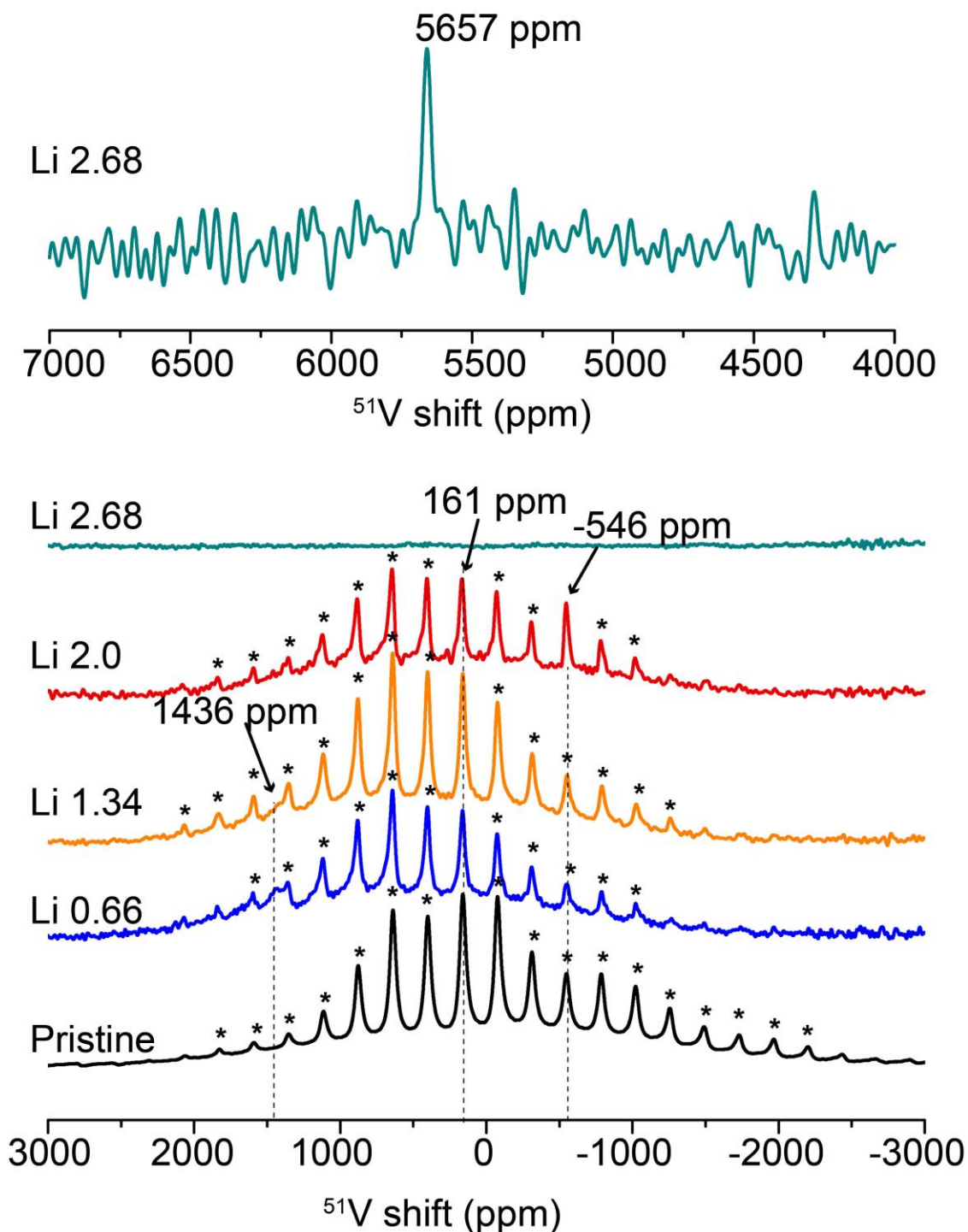
Figure 5. [51]V NMR spectra of VS$_4$-rGO acquired at 9.4 T during the first discharge curve for Li 0.66 – Li 2.68. The electrochemistry is as shown in Figure 4. The isotropic shifts are determined by measuring the spectra at two different spinning speeds (see supplemental figure, SI. 5) and are indicated by their isotropic shifts and dashed lines. The asterisks denote spinning side bands. The pristine spectrum was acquired at a different carrier frequency (O1) of ~-565 ppm compared to the other spectra (~200 ppm).
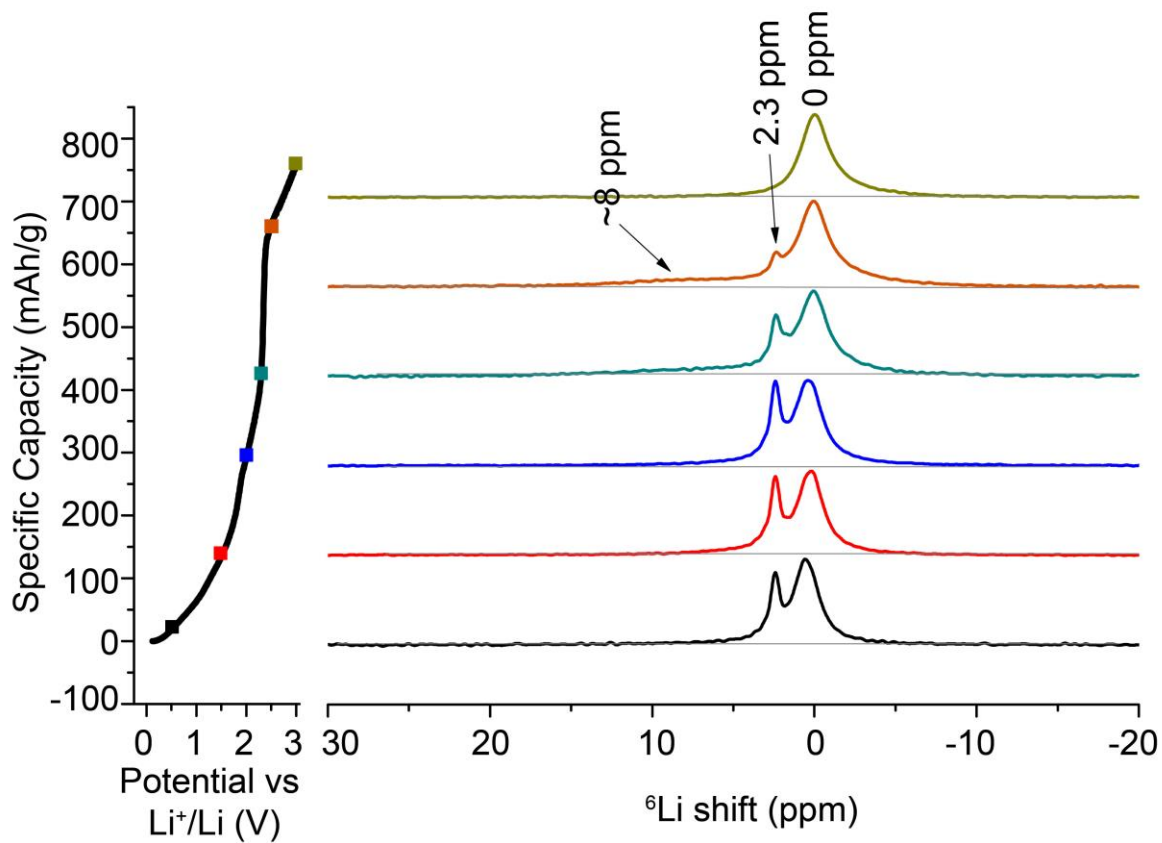
Figure 6. ^{6}Li NMR spectra of VS$_4$-GO during charge. The dashed baseline is shown so that the broader resonance at ~8 ppm can be seen more clearly.
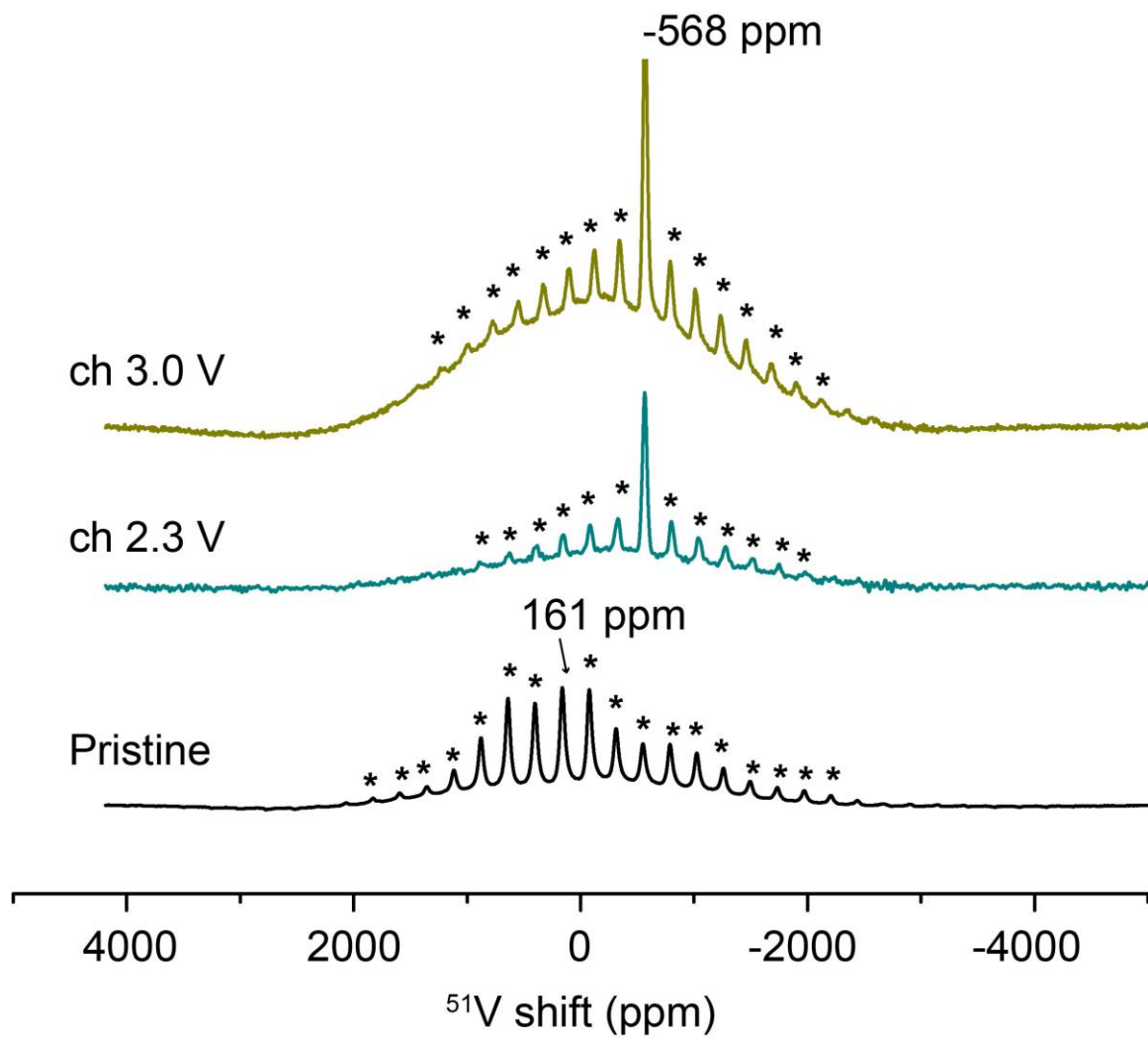
Figure 7. [51]V NMR of samples acquired during charging, acquired at 9.4 T. The resonance at -568 ppm has been truncated to show the lower intensity resonances more clearly.
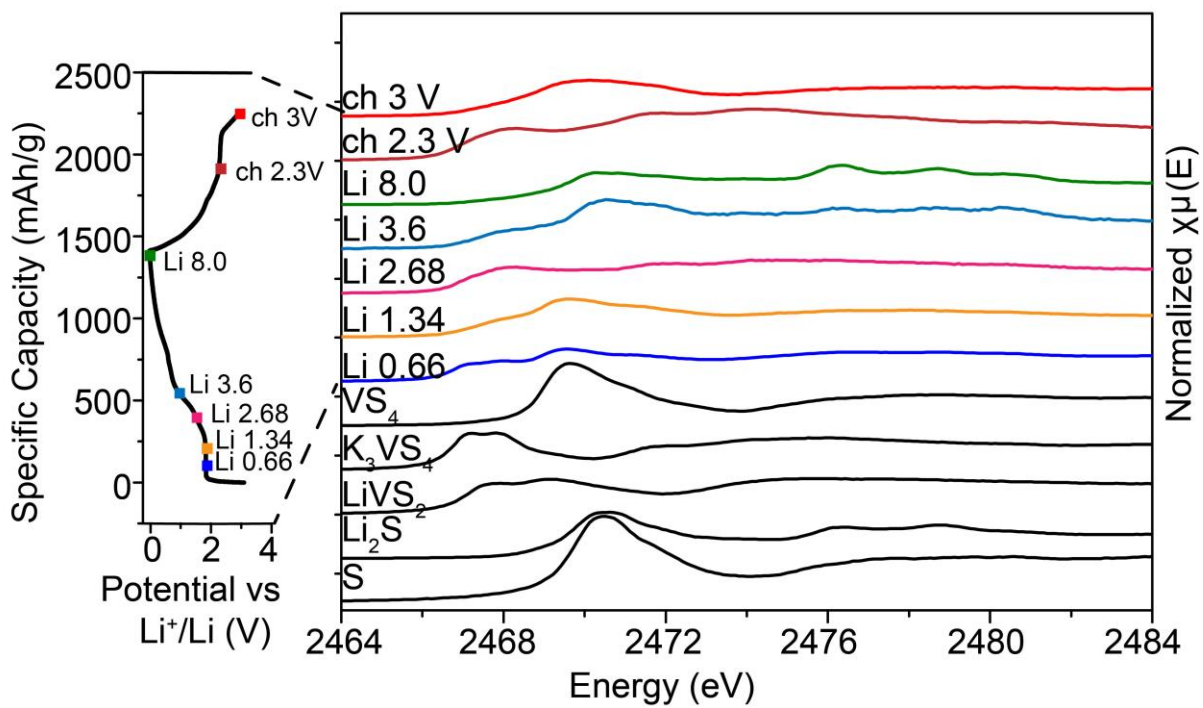
Figure 8. Normalized S K-edge XANES spectra of the model compounds and cycled VS$_4$-rGO samples.
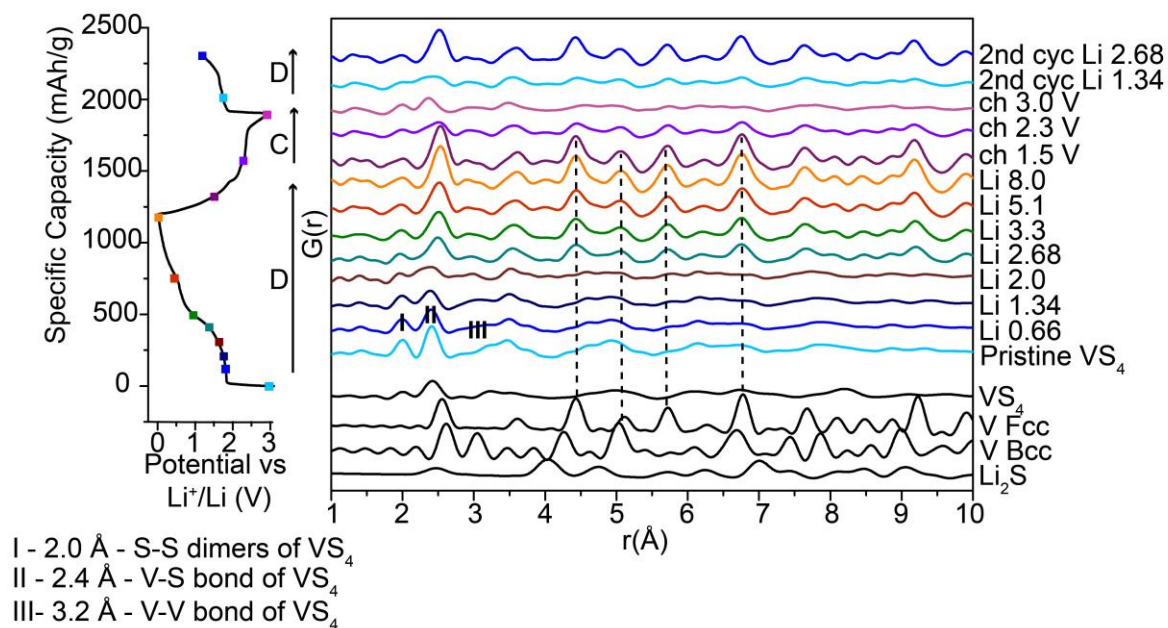
Figure 9. Ex-situ Pair Distribution Function data of VS_4-rGO samples. The simulated PDF patterns of the model compounds (VS_4, Li_2S, bcc and fcc V) are given at the bottom. The vertical lines correspond to fcc-V
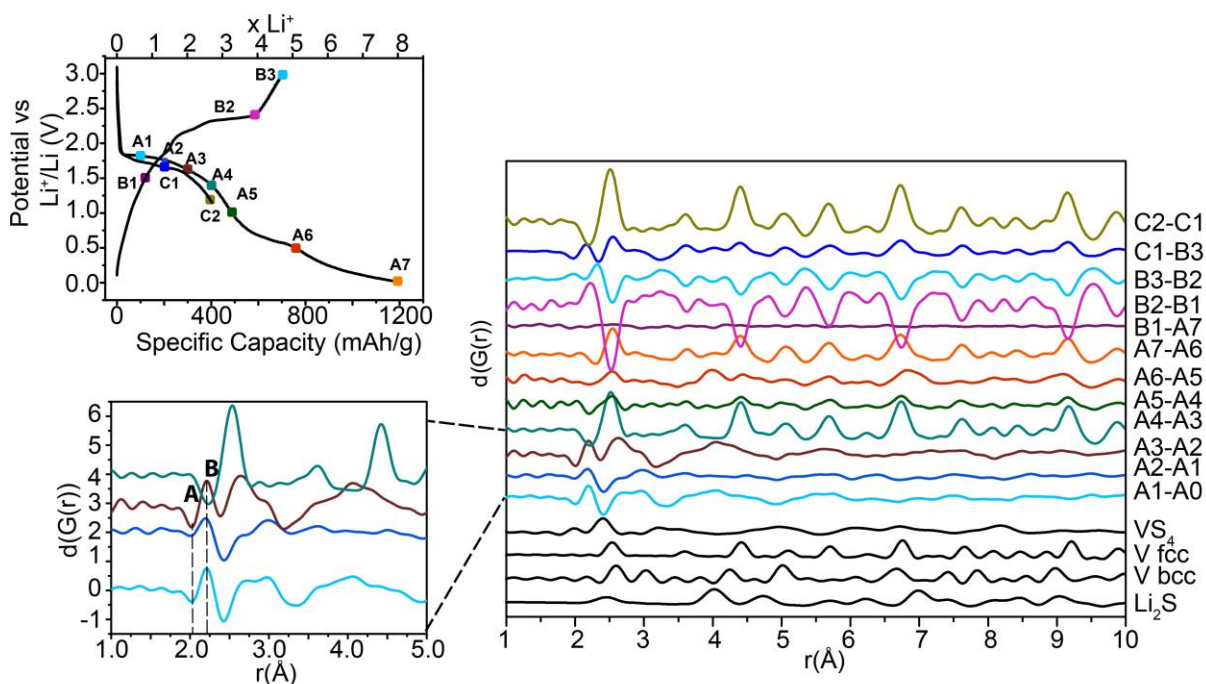

Figure 10. Ex-situ Difference PDF patterns of VS_4-rGO. A and B in the left lower side panel are referred to in the text.
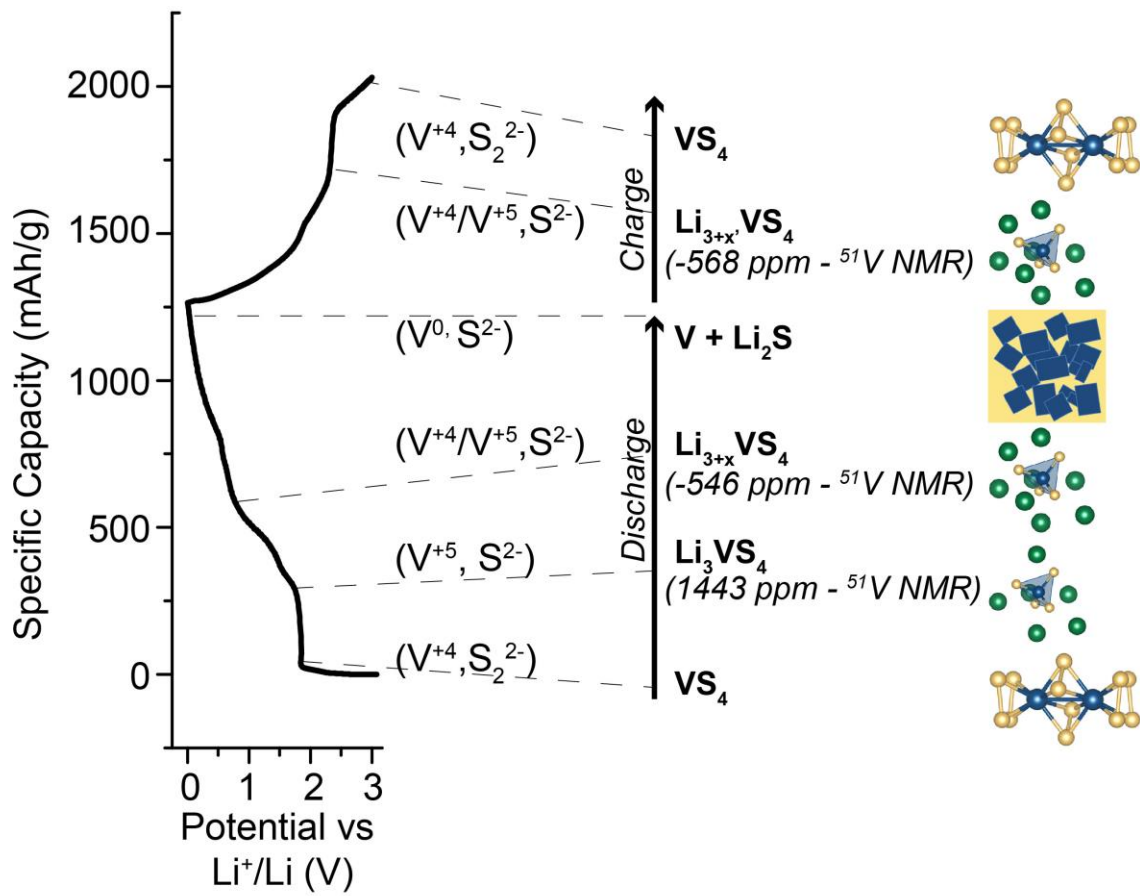
Figure 11. Summary of the redox processes occurring during discharge/charge of VS_4.